Radio Signals from Axion Dark Matter Conversion in Neutron Star Magnetospheres

Supplementary Material

Anson Hook, Yonatan Kahn, Benjamin R. Safdi, Zhiquan Sun

This Supplementary Material contains additional calculations and examples that support the results presented in the main Letter and further illustrate the phenomenology of a hypothetical signal. We begin by giving a heuristic derivation of the conversion probability that does not rely on having to solve the coupled differential equations but rather is based on more general physics arguments. We also give an extended derivation of the mixing equations and their solution, including the effects of strong magnetic fields in the plasma, along with numerical examples that support the analytic solution for the conversion probability used in the main Letter. Next, we discuss the non-trivial light curves and polarization profiles that might be expected from an axion signal. Finally, we describe how to estimate the radio sensitivity, accounting for the optimal bandwidth for an analysis of the radio data given knowledge of the DM velocity distribution and also knowledge of the non-trivial light curves, and highlight the strong angular dependence of the signal.

CONVERSION PROBABILITY PARAMETRICS

We first demonstrate how to understand the parametric dependence of the axion-photon conversion rate. Parametrically, the axion photon conversion rate is of the form

$$P(a \to \gamma) \sim \sin^2\Theta \sin^2(\Delta k L) \tag{S1}$$

where $\tan\Theta \sim B g_{a\gamma\gamma}\omega/(m_a^2 - m_\gamma^2)$ is the mixing between the axion and the photon, Δk is the difference in momentum between an axion and photon of the same energy, and L is the distance over which the conversion occurs. As is well known, relativistic axions converting in a magnetic field in vacuum have $m_\gamma = 0$ and $\Delta k \sim m_a^2/\omega$ so that $\Theta \ll 1$ and the conversion probability scales as

$$P(a \to \gamma) \sim \Theta^2 \Delta k^2 L^2 \sim B^2 g_{a\gamma\gamma}^2 L^2. \tag{S2}$$

This gives the conversion probability familiar from experiments such as CAST.

In this work, we consider the very different regime where axion-photon mixing is maximal due to $m_\gamma \sim m_a$, but the axion is non-relativistic. As a direct consequence of the assumption that the photon effective mass is the same as the axion mass, we have $\Theta \sim \mathcal{O}(1)$. When mixing is maximal, the difference in momentum between the two propagating eigenstates is $\Delta k \sim \frac{B\omega g_{a\gamma\gamma}}{k}$, where we are using (4) (or (S9) below) and ignoring any $\tilde{\theta}$ dependence for simplicity. Thus the conversion rate is given by

$$P(a \to \gamma) \sim \Delta k^2 L^2 \sim \frac{1}{v_c^2} B^2 g_{a\gamma\gamma}^2 L^2. \tag{S3}$$

Note that while (S3) is similar to (S2), the derivation and region of validity is completely different. For example, if the axions were assumed to be relativistic instead of non-relativistic, the conversion probability would instead be highly suppressed by the large magnetic fields of the NS [17]. Because NSs are macroscopic objects with large magnetic fields that extend over macroscopic distances, the length scale L is not determined by the change in the magnetic field, but instead by the change in the plasma frequency of the photon. Eq. (S3) assumes coherent conversion, i.e. that photons which were generated from conversion at r and $r + L$ add coherently. If the plasma mass changes over this distance, then photons generated at r_1 can instead interfere with photons generated at a different radius r_2. L is roughly the distance over which photons generated at the beginning start to interfere with photons generated at the end, i.e. $L \sim 1/\delta k$, where δk is the difference in momentum at different locations. $k\delta k \sim m_\gamma \delta m_\gamma$ and due to the power-law dependence of the photon effective mass on r, we also have $\delta m_\gamma/m_\gamma \sim L/r_c$. Thus we have the estimate that

$$L \sim \sqrt{\frac{r_c v_c}{m_a}}. \tag{S4}$$

The final axion photon conversion rate is

$$P(a \to \gamma) \sim \frac{B^2 g_{a\gamma\gamma}^2 r_c}{v_c m_a}. \tag{S5}$$

In the main Letter, and in more detail below, we carefully calculate the axion-photon conversion probability from the mixing equations, but the parametric scaling can be understood by the arguments just put forth.

AXION-PHOTON CONVERSION

In this section, we give additional details of the equations of motion of the axion-photon system and the approximate solution to these equations for axion DM in the NS magnetosphere.

Equations of motion

The plasma surrounding a NS is a cold, highly-magnetized plasma and due to the large magnetic field it is strongly birefringent. The effect of the magnetic field and plasma is taken into account by introducing a dielectric tensor. Because the photon has both transverse and longitudinal modes, it is convenient to work directly with the electric field. The propagation of electromagnetic waves and axions in a plasma is determined by

$$\begin{aligned} -\partial_t^2 a + \nabla^2 a &= m_a^2 a - g_{a\gamma\gamma}\mathbf{E}\cdot\mathbf{B}, \\ -\nabla^2\mathbf{E} + \nabla(\nabla\cdot\mathbf{E}) &= \omega^2\mathbf{D} + \omega^2 g_{a\gamma\gamma} a\mathbf{B}, \end{aligned} \tag{S6}$$

where the magnetic field $\mathbf{B}$ is taken to be the external magnetic field due to the NS. We work over a small enough region of space where the change in gravitational potential may be neglected. The electric displacement field $\mathbf{D}$ is given by [51]

$$\mathbf{D} = R^{yz}_{\tilde{\theta}} \cdot \begin{pmatrix} \epsilon & ig & 0 \\ -ig & \epsilon & 0 \\ 0 & 0 & \eta \end{pmatrix} \cdot R^{yz}_{-\tilde{\theta}} \cdot \begin{pmatrix} E_x \\ E_y \\ E_z \end{pmatrix}, \tag{S7}$$

where the magnetic field is taken to be at an angle $\tilde{\theta}$ from the z-axis in the positive $y-z$ quadrant, and $R^{yz}_{\tilde{\theta}}$ is the rotation matrix by $\tilde{\theta}$ in the yz-plane. The coefficients in the dielectric tensor are given by

$$\epsilon = 1 - \frac{\omega_p^2}{\omega^2 - \Omega_c^2} \qquad g = \frac{\omega_p^2 \Omega_c}{\omega(\omega^2 - \Omega_c^2)} \qquad \eta = 1 - \frac{\omega_p^2}{\omega^2} \qquad \omega_p = \frac{4\pi\alpha n_e}{m_e} \qquad \Omega_c = \frac{\sqrt{\alpha}B}{m_e}\,. \tag{S8}$$

Taking the Fourier transform in time, and going to the high-magnetization limit ($\Omega_c \gg \omega, \omega_p$), which sends $\epsilon \to 1$ and $g \to 0$, E_x decouples from the equations, and E_z does not propagate and can be solved for algebraically. The mixing matrix simplifies to

$$-\partial_z^2 \begin{pmatrix} E_y \\ a \end{pmatrix} = \begin{pmatrix} \frac{\omega^2 - \omega_p^2}{1 - \frac{\omega_p^2}{\omega^2}\cos^2\tilde{\theta}} & \frac{g_{a\gamma\gamma} B_t \omega^2}{1 - \frac{\omega_p^2}{\omega^2}\cos^2\tilde{\theta}} \\ \frac{g_{a\gamma\gamma} B_t}{1 - \frac{\omega_p^2}{\omega^2}\cos^2\tilde{\theta}} & \omega^2 - m_a^2 \end{pmatrix} \cdot \begin{pmatrix} E_y \\ a \end{pmatrix}, \tag{S9}$$

where $B_t = |\mathbf{B}|\sin\tilde{\theta}$ is the component of the B-field transverse to the direction of motion. Equation (4) is derived from a WKB approximation of this second-order differential equation, assuming outgoing plane waves in the radial direction with a local coordinate system defined by $\hat{\mathbf{r}} = \hat{\mathbf{z}}$ and defining $A_\parallel = E_y/i\omega$.

Note that in (S9), we have neglected the vacuum birefringence term from strong-field QED. Ref. [17] points out that this term can drastically affect the axion-photon conversion probability; however, this term is negligible for non-relativistic DM axions. Vacuum birefringence changes the condition for resonance from $\omega_p = m_a$ to

$$\omega_p^2 - \frac{7}{2}\omega^2\kappa\sin^2\tilde{\theta} = m_a^2, \tag{S10}$$

where

$$\kappa = \frac{\alpha}{45\pi}\left(\frac{B}{B_{\rm crit}}\right)^2 \tag{S11}$$

determines the strength of vacuum birefringence effects. The critical field is

$$B_{\rm crit} = \frac{m_e^2}{e} \approx 4.4 \times 10^{13}\ {\rm G}. \tag{S12}$$

Ref. [17] points out that for sufficiently large κ and ultrarelativistic axions with $\omega \gg m_a$, the maximal mixing condition (S10) can never be satisfied because the left-hand side becomes negative. Fortunately, for nonrelativistic or mildly relativistic axions with $\omega = \mathcal{O}(1) \times m_a$, this is never a problem. Indeed, in this case we have

$$\frac{7}{2}\omega^2 \kappa \sin^2\tilde{\theta} \sim m_a^2 \times 10^{-4} \left(\frac{B}{4.4\times 10^{13}\ {\rm G}}\right)^2. \tag{S13}$$

Even for the largest NS magnetic fields considered in the Letter, the effects of the vacuum birefringence term are a percent-level perturbation and can be neglected for semi-relativistic axions, and $\omega_p = m_a$ can always be satisfied. More specifically, as long as $B \lesssim 10^{15}$ G (the size of the largest known magnetar fields), the maximal mixing conditions can always be satisfied, but for these large fields one would need to consider the effect of κ when solving for r_c.

Modulation of the photon wave

As mentioned in the main Letter, it is important to take into account the modulation of the outgoing electromagnetic wave in calculating the energy transfer from the axion field to the outgoing electromagnetic radiation. To isolate this effect, we neglect the mixing terms and consider the photon wave equation with a spatially-dependent plasma mass:

$$\frac{d^2}{dr^2}A_\parallel + \left(\omega^2 - \omega_p^2(r)\right) A_\parallel = 0\,. \tag{S14}$$

We now define $k(r) = \sqrt{\omega^2 - \omega_p^2(r)}$ and use a second WKB approximation, performing an expansion in the small dimensionless parameter $\varepsilon = \frac{1}{k^2}\frac{dk}{dr}$. We have verified that this parameter is small for $r > r_c$. This gives the solution (for $r > r_c$)

$$A_\parallel(r,t) = \frac{c}{\sqrt{k(r)}} e^{i\omega t - i\int_{r_c}^{r} k(r')dr'}. \tag{S15}$$

Solving (4) for the photon field leads to the expression in (7).

The axion-photon evolution at finite r

In the main Letter, we presented an approximate expression for the energy transfer function at infinity $p_{a\gamma}^{\infty}$. In this subsection, we give the result for $F_{a\gamma} \equiv |A_\parallel(r)|^2/a_0^2$ at finite r. First, we consider $\tilde{\theta} = \pi/2$, where $\tilde{\theta}$ is the angle between the B-field and $\hat{\mathbf{r}}$, and then we discuss the generalization to arbitrary $\tilde{\theta}$. Taking $\tilde{\theta} = \pi/2$ and performing the integral in (7) at finite r, we find

$$\begin{aligned} F_{a\gamma}(r) \approx{}& \frac{1}{2v_c^2}\, g_{a\gamma\gamma}^2 B(r_c)^2 L^2 \times G\left(\frac{r-r_c}{L}\right) \\ &\times \begin{cases} 1, & r < r_c \\ \frac{m_a v_c}{k(r)}, & r \geq r_c \end{cases}, \end{aligned} \tag{S16}$$

with $L = \sqrt{2\pi r_c v_c/(3m_a)}$ and the function $G(x)$ defined by

$$G(x) = \frac{\left(\frac{1}{2} + C(x)\right)^2 + \left(\frac{1}{2} + S(x)\right)^2}{2} \tag{S17}$$

in terms of the Fresnel C and S integrals. Note that $\lim_{x\to\infty} G(x) = 1$ and that $G\left(\frac{r-r_c}{L}\right)$ rises quickly from 0 at $r < r_c$ to values near unity at $r \sim r_c$, over a distance of order L, while the amplitude modulation of the outgoing wave is encapsulated by the second line in (S16).

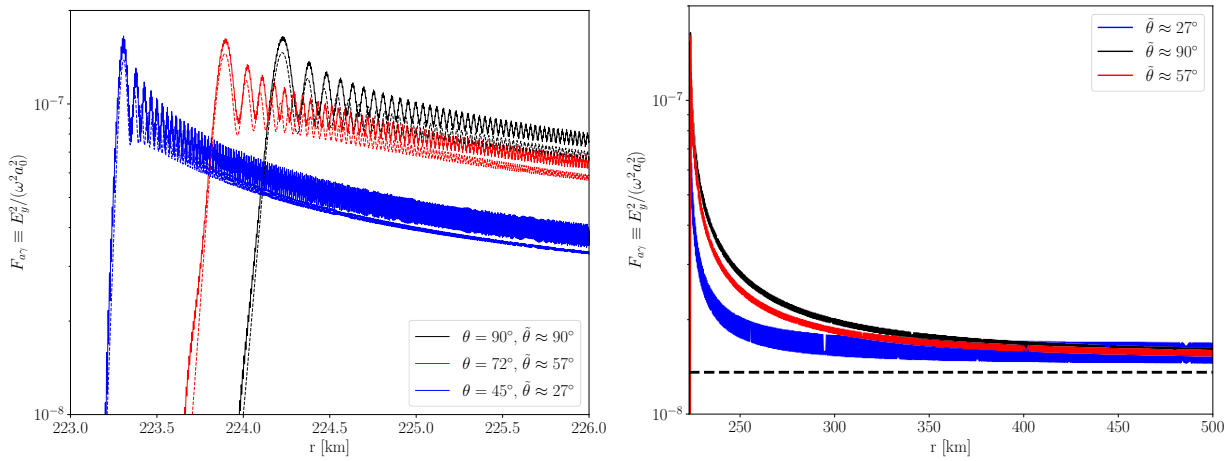

Figure S1. Energy transfer function from axions to photons as a function of the radius r from the NS center, for parameters $r_0 = 10$ km, $M_{\rm NS} = 1\,M_\odot$, $B_0 = 10^{14}$ G, $\theta_m = 0$, $P = 1$ sec, $m_a = 1$ GHz, and $g_{a\gamma\gamma} = 10^{-12}$ GeV^{-1}. Three different angles θ are shown, along with their corresponding angles $\tilde{\theta}$ between $\hat{\mathbf{r}}$ and the magnetic field. *(Left)* The solid curves show the numerical solutions for $F_{a\gamma}$ while the dashed illustrate the analytic approximation, for r near the conversion radius. *(Right)* As in the left panel, except over a wider range of r and only illustrating the numerical solutions (solid) and the asymptotic approximation $p_{a\gamma}^\infty$ (black, dashed) at $r \to \infty$, which is the same for all $\tilde{\theta}$ to leading order in v_c.

At arbitrary $\tilde{\theta}$, the length L, which is found from the stationary phase approximation to the integral in (6), is modified to

$$L'(\tilde{\theta}) = L\left(\tilde{\theta} = \frac{\pi}{2}, r_c'\right) \times \frac{\sin\tilde{\theta}\sqrt{1+v_c^2}}{\sqrt{1+v_c^2\sin^2\tilde{\theta}}}\,, \tag{S18}$$

and we should also make the substitution in (S16)

$$B'(\tilde{\theta}, r_c) = B(\tilde{\theta} = \frac{\pi}{2}, r_c') \times \frac{1+v_c^2\sin^2\tilde{\theta}}{\sin\tilde{\theta}(1+v_c^2)}\,. \tag{S19}$$

Moreover, the conversion radius r_c is modified to

$$r_c' = r_c \times \left(\frac{1+v_c^2\sin^2\tilde{\theta}}{1+v_c^2}\right)^{1/3}\,. \tag{S20}$$

Note that $B(r_c)^2L^2$, the quantity which appears in $F_{a\gamma}(r)$ and $p_{a\gamma}^\infty$, has no explicit dependence on $\tilde{\theta}$ up to $\mathcal{O}(v_c^2)$ corrections.

In Fig. S1, we compare our analytic estimate (S16) to numerical solutions to the full 2$^{\rm nd}$-order mixing equations in (S9), with boundary conditions imposed at $r = 223.05$ km ($r = 223.5$ km) for the blue (black and red) curves. We take the frequency $\omega \approx m_a(1 + \frac{1}{2}v_c^2)$, where v_c is the DM velocity at the conversion radius. In this example, we take $r_0 = 10$ km, NS mass $M_{\rm NS} = 1\,M_\odot$, $B_0 = 10^{14}$ G, $\theta_m = 0$, $P = 1$ sec, $m_a = 1$ GHz, and $g_{a\gamma\gamma} = 10^{-12}$ GeV^{-1}. This implies that the transition radius is at $r_c \approx 224$ km and that at this radius the axion velocity is $v_c \approx 0.11$, in natural units, where we neglect the $\mathcal{O}(10^{-3})$ initial axion velocity v_0 asymptotically far away from the NS. We illustrate three different angles, $\theta = 90°$, $72°$, and $45°$; for each angle, the angle $\tilde{\theta}$ between $\hat{\mathbf{r}}$ and the magnetic field is indicated in the figure. As we change θ, we change the conversion radius r_c given in (3) because of the angular dependence of the plasma frequency. However, in order to highlight the differences between the different $\tilde{\theta}$ we chose to fix the normalization of the plasma frequency to that found at $\theta = 90°$. That is, at the level of the equations of motion in (S9), we keep the implicit dependence of ω_p on θ fixed and only vary the explicit dependence of $\tilde{\theta}$. In the left panel, the solid curves show the numerical solutions for $F_{a\gamma} \equiv E_y^2/(\omega^2 a_0^2)$, while the dashed show the analytic approximations, which are seen to agree well. Indeed, we see that both the peak values and the asymptotic values for both the analytical and numerical solutions are independent of $\tilde{\theta}$ (and hence θ). This is further illustrated in the right panel, where we compare the numerical solutions to the energy transfer function $p_{a\gamma}^\infty$ (black, dashed), which is the same for all $\tilde{\theta}$ to leading order in v_c.

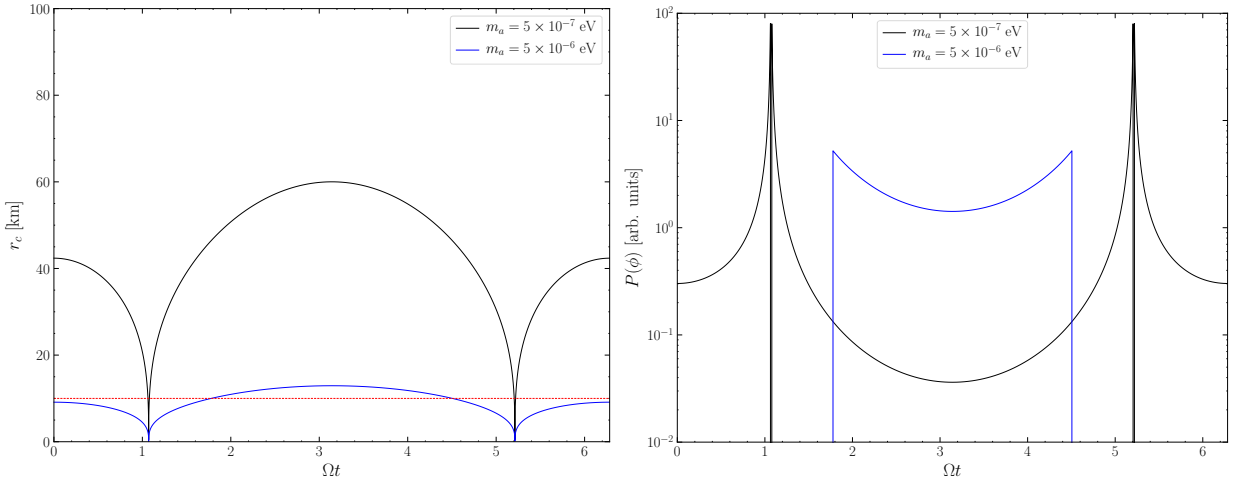

Figure S2. (*Left*) The conversion radius as a function of the phase Ωt for RX J0806.4-4123 assuming $\theta_m = 15^\circ$ and $\theta = 45^\circ$, for two different axion masses. (*Right*) The radiated power for the setup in the left panel, in arbitrary units, as a function of the phase. The radiation stops when the conversion radius falls below the radius of the NS, which is indicated by the dashed red line in the left panel.

We note that there are small discrepancies between the analytic approximation (7) and the numerical solutions in these examples. These may be due in part to the necessity of setting the boundary conditions very close to r_c rather than at r_0 to avoid contamination of the solution by the spurious exponentially-growing mode when $\omega < \omega_p$. Still, the difference between the analytic and numerical results is less than $\sim 10\%$ at large r.

LIGHT CURVES AND POLARIZATIONS

The misalignment between the pulsar's magnetic axis and rotation axis leads to non-trivial light curves. Fig. S2 shows the change in the conversion radius and the radiated power over the pulsar's rotation period as a function of the rotation phase for an example NS.

The misaligned NS also leads to non-trivial polarization structure. This is because the electric field of the radio emission is aligned with the tangential component B_t of the NS's magnetic field, but the direction of B_t changes as a function of Ωt. A more careful analysis is needed to verify if the polarization structure survives Faraday rotation induced from the magnetosphere, but we neglect this effect for now and study the polarization of the photons as they are emitted. We define the basis vectors $\hat{\epsilon}_{\mathbf{1}} = \hat{\theta}$ and $\hat{\epsilon}_{\mathbf{2}} = \hat{\phi}$ for the polarization, where $\hat{\theta}$ and $\hat{\phi}$ are the polar and azimuthal unit vectors in the NS's frame. Without loss of generality, we may consider the Earth to be at $\phi = 0$ in the frame of the NS, such that $\hat{\mathbf{m}} \cdot \hat{\mathbf{r}} = \cos\theta_m \cos\theta + \sin\theta_m \sin\theta \cos(\Omega t)$. The time-dependent polarization vector $\hat{\mathbf{n}}(t)$ of the radio emission is given by

$$\hat{\mathbf{n}}(t) = \frac{\big(\cos\theta_m \sin\theta - \sin\theta_m \cos\theta \cos(\Omega t)\big)\hat{\epsilon}_{\mathbf{1}} - \sin\theta_m \sin(\Omega t)\hat{\epsilon}_{\mathbf{2}}}{\sqrt{\big(\cos\theta_m \sin\theta - \sin\theta_m \cos\theta \cos(\Omega t)\big)^2 + \sin^2\theta_m \sin^2(\Omega t)}}\,. \tag{S21}$$

In Fig. S3, we illustrate the linear polarization profiles, neglecting the possible effect of Faraday rotation, in the $\hat{\epsilon}_{\mathbf{1}}$ and $\hat{\epsilon}_{\mathbf{2}}$ directions over a pulsar period. Note that for $\theta = 90^\circ$ and a small misalignment angle $\theta_m = 15^\circ$, the outgoing wave is almost completely polarized over the whole rotation period.

RADIO SENSITIVITY ESTIMATES

In this section we give additional details for how we make the radio sensitivity estimates in the main Letter.

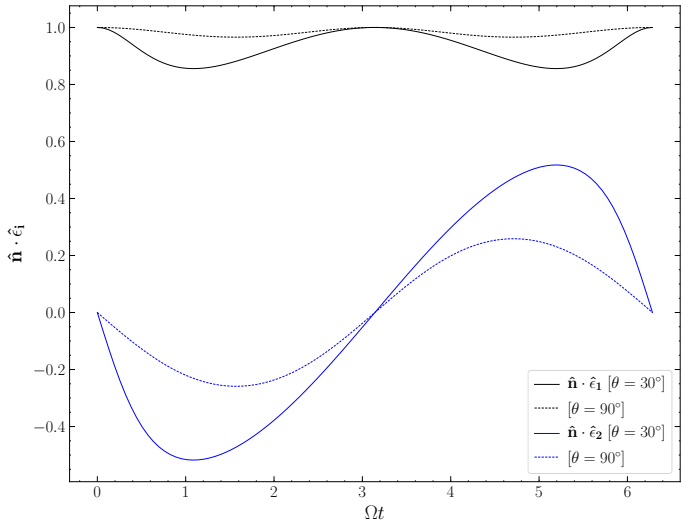

Figure S3. The $\hat{\epsilon}_1$ (black) and $\hat{\epsilon}_2$ (blue) polarization components of the electric field as a function of the phase Ωt for various θ, with $\theta_m = 15°$. Note that these polarization curves are valid for any NS with these alignments, though depending on m_a and the NS properties, the NS may not radiate over the whole period since r_c may drop below the conversion radius (see Fig. S2).

Bandwidth optimization

Considering that the asymptotic DM velocities, which determine the spread of photon frequencies, have a dispersion $\sim v_0$, it follows that we expect the bandwidth B of the radio signal to be $B \sim m_a v_0^2/(2\pi)$, where the 2π simply arises from the translation from angular frequency. However, it is worth calculating the optimal bandwidth for an analysis of the radio-telescope data given that we are trying to optimize SNR $\sim \sqrt{B}S \sim F/\sqrt{B}$. Having a smaller bandwidth increase our signal-to-noise ratio because of the $\sqrt{B}$ in the denominator, but on the other hand this also means that we have less flux F, which acts to decrease the signal. In this section, we compute the optimal bandwidth by maximizing $F/\sqrt{B}$.

Let us define

$$I(\omega_1, \omega_2) \equiv \frac{\int_{\omega_1}^{\omega_2} d\omega f_\omega(\omega)}{([\omega_2 - \omega_1]/2\pi)^{1/2}}\,, \tag{S22}$$

where $I(\omega_1, \omega_2)$ is the function to maximize and where $f_\omega(\omega)$ is the distribution of radio frequencies in the lab-frame for an axion signal with mass m_a. In the DM frame, the DM velocity distribution is given by (9). Let us assume that the NS is boosted with a velocity $\mathbf{v}_\mathrm{b}$ with respect to the DM frame. Then, the distribution of frequencies in the NS frame, but asymptotically far away from the NS, is given by

$$f_\omega(\omega) = \frac{2}{\sqrt{\pi} m_a v_b v_0} e^{\frac{2 - v_b^2 - 2\tilde{\omega}}{v_0^2}} \sinh\left(\frac{2 v_b \sqrt{2\tilde{\omega} - 2}}{v_0^2}\right)\,, \tag{S23}$$

where we have defined $\tilde{\omega} \equiv \omega/m_a$. This implies that

$$\begin{aligned} I(\omega_1, \omega_2) = \sqrt{\frac{2\pi}{m_a v_0^2}} \frac{1}{\tilde{B}^{1/2}} \frac{1}{2} \Big[&-2 + \mathrm{erf}\big(x - \sqrt{2}\sqrt{\delta\tilde{\omega}_1}\big) + \mathrm{erf}\big(x + \sqrt{2}\sqrt{\delta\tilde{\omega}_2}\big) + \mathrm{erfc}\big(x + \sqrt{2}\sqrt{\delta\tilde{\omega}_1}\big) \\ &+ \mathrm{erfc}\big(x - \sqrt{2}\sqrt{\delta\tilde{\omega}_2}\big) + 2e^{-x^2} \frac{e^{-2\delta\tilde{\omega}_1} \sinh(2\sqrt{2\delta\tilde{\omega}_1} x) - e^{-2\delta\tilde{\omega}_2} \sinh(2\sqrt{2\delta\tilde{\omega}_2} x)}{\sqrt{\pi} x} \Big]\,, \end{aligned} \tag{S24}$$

with $x \equiv v_b/v_0$ and $\omega_{1,2} = m_a + m_a \delta\tilde{\omega}_{1,2} v_0^2$. We have also defined $B \equiv (\omega_2 - \omega_1)/2\pi$ and $\tilde{B} \equiv 2\pi B/(m_a v_0^2)$. For $x = 0$, we find the maximum at $\tilde{\delta}\omega_1 = 0.013$ and $\tilde{B}^* \approx 1.12$, with value $I(w_1, w_2)\sqrt{m_a v_0^2/(2\pi)} \approx 0.74$. For $x = 1$, we find the maximum at $\tilde{\delta}\omega_1 = 0.032$ and $\tilde{B}^* \approx 1.97$, with value $I(w_1, w_2)\sqrt{m_a v_0^2/(2\pi)} \approx 0.58$.

Some explanation is warranted here. First, we have not accounted for the gravitational potential of the NS for the reason mention in the main Letter: a DM wave with energy ω asymptotically far away from the NS will produce an

electromagnetic wave of frequency ω when measured asymptotically far from the NS, since both the axion-photon mixing equations and the NS's gravitational potential conserve energy. Second, we have not accounted for the boost of the lab frame with respect to the NS because this boost only affects the radio emission; such small boosts are not important for relativistic particles. On the other hand, the NS boost with respect to the DM distribution is important because DM is non-relativistic.

Time-dependent light curves

Any analysis of real radio data for evidence of a DM signal will likely proceed through the use of a non-trivial likelihood function that properly accounts for the expected statistics of the observable, which may be the power within a frequency bin, under the null and signal hypotheses. However, if we assume that the power measurements are normally distributed, we may write down a simple chi-square statistic that allows us to quickly estimate the sensitivity to axion signals with non-trivial light curves. In particular, we may write

$$\chi^2 = \sum_{i=1}^{N_f} \sum_{j=1}^{N_t} \frac{(S_{i,j} - S_b)^2}{\sigma_{S_b}^2}\,, \tag{S25}$$

where i labels the different independent frequency bins and j labels the independent time bins. Here, $S_{i,j}$ is the measured flux density within bin (i,j), and S_b is the predicted mean background flux density under the null hypothesis. Note that we assume that S_b is independent of (i,j), though including dependence on the frequency and on time does not modify the main conclusion of this section. Similarly, $\sigma_{S_b}^2$ is the expected variance of the flux density in a single bin under the null hypothesis. Assuming the null hypothesis arises from thermal noise in the telescope, we may write

$$\sigma_{S_b} = \frac{\mathrm{SEFD}}{\sqrt{n_{\mathrm{pol}} df dt}}\,, \tag{S26}$$

where df (dt) is the frequency (time) spacing between frequency (time) bins.

To estimate the mean expected significance of an axion signal, we follow the Asimov framework [52] and take the data to be equal to the mean dataset under the signal hypothesis: $S_{i,j} = S_b + S_{i,j}^{\mathrm{axion}}$, where $S_{i,j}^{\mathrm{axion}}$ is the mean contribution from the axion in bin (i,j). Then, we find

$$\chi^2_{\mathrm{Asimov}} = \frac{n_{\mathrm{pol}}}{\mathrm{SEFD}^2} \sum_{i=1}^{N_f} df \sum_{j=1}^{N_t} dt\, (S_{i,j}^{\mathrm{axion}})^2\,. \tag{S27}$$

The signal will, roughly, have support over a range of frequencies of width equal to the bandwidth B, discussed in the previous subsection, so that we may write

$$\chi^2_{\mathrm{Asimov}} = \frac{n_{\mathrm{pol}} B}{\mathrm{SEFD}^2} \sum_{j=1}^{N_t} dt\, (S_{j}^{\mathrm{axion}})^2\,. \tag{S28}$$

A more careful likelihood function that includes the expected line-shape of the signal may be slightly more sensitive to a putative axion signal, but the development of such a likelihood is beyond the scope of the current work and not the focus of the current subsection. We may write

$$S_j^{\mathrm{axion}} = S_0 \times f(j \times dt)\,, \tag{S29}$$

where

$$S_0 = 6.7 \times 10^{-5}\ \mathrm{Jy} \left(\frac{100\ \mathrm{pc}}{d}\right)^2 \left(\frac{1\ \mathrm{GHz}}{m_a}\right) \left(\frac{200\ \mathrm{km/s}}{v_0}\right)^2 \left[\frac{d\mathcal{P}(\theta = \frac{\pi}{2}, \theta_m = 0)/d\Omega}{4.5 \times 10^8\ \mathrm{W}}\right]\,, \tag{S30}$$

and

$$f(t) = \frac{3\,(\hat{\mathbf{m}} \cdot \hat{\mathbf{r}})^2 + 1}{\left|3 \cos\theta\, \hat{\mathbf{m}} \cdot \hat{\mathbf{r}} - \cos\theta_m\right|^{4/3}} \Theta(r_c(t) - r_0) \tag{S31}$$

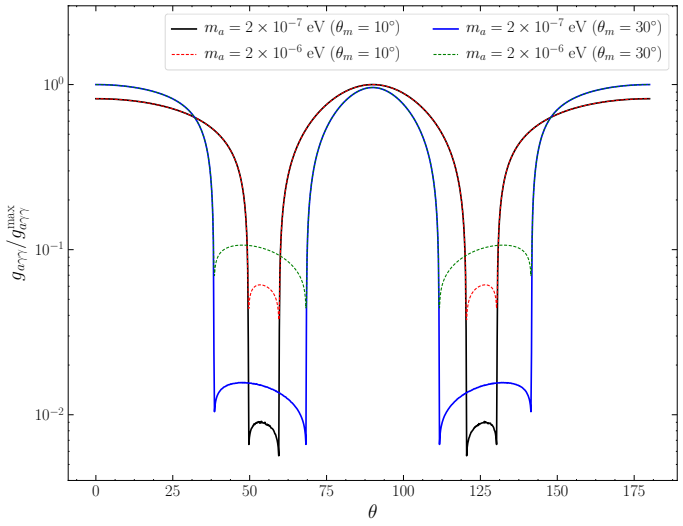

Figure S4. Sensitivity to $g_{a\gamma\gamma}$ for two different axion masses m_a and two different misalignment angles θ_m, as a function of θ, the polar angle of the Earth in the frame of the NS. The remaining parameters, chosen for illustration, are $B_0 = 2.5\times10^{13}$ G, $P = 1$ s, and $r_0 = 10$ km. Smaller values of $g_{a\gamma\gamma}/g_{a\gamma\gamma}^{\rm max}$ indicate an enhancement.

with $\hat{\mathbf{m}}\cdot\hat{\mathbf{r}}$ and $r_c(t)$ functions of time. Then, we see that

$$\begin{aligned}\chi^2_{\rm Asimov} &= \frac{n_{\rm pol}B}{\rm SEFD^2}S_0^2\int_0^{\Delta t_{\rm obs}} dt\,[f(t)]^2 \\ &= \frac{n_{\rm pol}B\Delta t_{\rm obs}}{\rm SEFD^2}S_0^2\frac{\int_0^{2\pi}d\phi\,[f(\phi)]^2}{2\pi}\,,\end{aligned} \tag{S32}$$

where $\Delta t_{\rm obs}$ is the total time the radio telescope observed, and ϕ is the azimuthal coordinate on the NS. That is,

$$\begin{aligned}\hat{\mathbf{m}}\cdot\hat{\mathbf{r}} &= \cos\theta_m\cos\theta + \sin\theta_m\sin\theta\cos(\phi)\,, \\ r_c(\phi) &= 224\text{ km}\times\left(\frac{r_0}{10\text{ km}}\right)\left[\frac{B_0}{10^{14}\text{ G}}\,\frac{1\text{ sec}}{P}\left(\frac{1\text{ GHz}}{m_a}\right)^2\right]^{1/3}|3\cos\theta\,\hat{\mathbf{m}}\cdot\hat{\mathbf{r}} - \cos\theta_m|^{1/3}\,,\end{aligned} \tag{S33}$$

where we can also identify $\phi = \Omega t$. Evaluating (S32) and solving for $g_{a\gamma\gamma}$ such that $\chi^2_{\rm Asimov} = 1$ leads to the projected sensitivities in Fig. 1.

Angular dependence of sensitivity

In Fig. 1 we showed the projected sensitivity to $g_{a\gamma\gamma}$ as a function of mass for two different angles θ, with $\theta_m = 10°$. However, it is important to understand how the sensitivity changes a function of θ, given that in practice this will be a random angle that depends on the relative orientation of the Earth and the NS being observed. In Fig. S4 we show how the sensitivity changes as a function of θ for the two cases $\theta_m = 10°,\ 30°$. We illustrate two different masses, $m_a = 2\times10^{-7}$ eV and $m_a = 2\times10^{-6}$ eV, and normalize the sensitivity to the maximum (worst) value, $g_{a\gamma\gamma}^{\rm max}$, found over all θ. Note that the large enhancement due to the strong beaming is found over a relatively wide range of θ, so we may expect such an enhancement for generic NS targets.

Additional sources of frequency broadening

In this Letter and in the discussions above specifically, we assumed that the bandwidth of the signal is set by the asymptotic velocity dispersion of DM. In this subsection we investigate other possible sources of frequency broadening. In particular, we discuss what we believe to be the next most important source of frequency broadening due to the

acceleration of the plasma. As we will show, the acceleration-induced broadening is sub-dominant compared to that from the asymptotic DM velocity spread.

It is well known that the indices of refraction of media are a function of the laboratory-frame boost of the media under question [53]. This effect can make media appear to have anisotropic refraction index tensors when boosted, even when the media have isotropic indices of refraction in their rest frame. The plasma frequency discussed in this Letter in the NS magnetosphere can be thought of as an index of refraction, and in the GJ model the plasma is boosted because it co-rotates with the NS. The effect of this boost is to give a small perturbation to the plasma frequency and thus the conversion radius, though this makes a negligible difference to the radiated power.

While the effect described above, due to the finite velocity of the magnetosphere, does not by itself broaden the frequency spectrum of the line, the line is broadened by the fact that the magnetosphere is accelerating. The reason for this induced line-width arises from the following physical mechanism. Consider a monochromatic electromagnetic beam, propagating in the $\hat{\mathbf{x}}$ direction, that encounters a block of index of refraction n that is accelerating with acceleration of magnitude a in the $\hat{\mathbf{x}}$-$\hat{\mathbf{y}}$ plane at an angle θ from the $\hat{\mathbf{x}}$ axis. Independent of the angle θ, we let the beam propagate a length δx through the medium before exiting back into vacuum. The beam will experience a frequency shift δf upon exiting the medium, with [54]

$$\frac{\delta f}{f} = a\cos(\theta)(n-1)\delta x\,. \tag{S34}$$

The fact that $\delta f \to 0$ as $\theta \to \pi/2$ is due to symmetry, since if the medium is accelerating perpendicular to the beam, then there is no preferred direction for the frequency shift. It is important to emphasize, also, that beams do not acquire frequency shifts when propagating through boosted media that are not accelerated. This is due to conservation of energy. For boosted but not accelerating media, energy is conserved because of time-translation invariance. However, when we introduce acceleration, energy is not conserved and so we should not expect the frequencies to leave the media unchanged.

We now apply (S34) to the problem of electromagnetic radiation propagating through the accelerating NS magnetosphere. The acceleration, at any radius r, is $a = \omega_{\rm NS}^2 r$, where $\omega_{\rm NS}$ is the NS's rotational frequency, and the acceleration vector is always in the $\hat{\theta} - \hat{\phi}$ plane, regardless of the angle between the NS's rotation and magnetic axes. We consider an electromagnetic wave produced from axion-photon conversion as the conversion radius r_c propagating to distances asymptotically far away from the NS. To leading order, the radiation travels along radial trajectories and thus does not experience a frequency shift from the acceleration. More precisely, we can expect $a\cos(\theta)$, in the language of (S34), to be approximately $a \times (v_{\rm DM}^\infty/v_c)$ in the vicinity of the conversion radius, where $v_{\rm DM}^\infty$ is the asymptotic DM velocity and v_c is the escape velocity at the conversion radius. This is simply the statement that the electromagnetic waves will deviate from radial trajectories at the level $v_{\rm DM}^\infty/v_c \sim 10^{-2}$. Within the GJ model, the index of refraction for $r > r_c$ is given by

$$n(r) = \frac{1}{\sqrt{1-\left(\frac{r_c}{r}\right)^3}}\,. \tag{S35}$$

This then implies that the total frequency shift is

$$\begin{aligned}\frac{\Delta f}{f} \equiv \frac{1}{f}\int_{r_c}^{\infty}\frac{df}{dr}dr &\approx \frac{v_{\rm DM}^\infty}{v_c}\omega_{\rm NS}^2\int_{r_c}^{\infty}\left(\frac{1}{\sqrt{1-\left(\frac{r_c}{r}\right)^3}}-1\right)r dr \\ &\approx 4\times 10^{-10}\left(\frac{0.1}{v_c}\right)\left(\frac{v_{\rm DM}^\infty}{10^{-3}}\right)\left(\frac{10\text{ s}}{P}\frac{r_c}{100\text{ km}}\right)^2\,.\end{aligned} \tag{S36}$$

This leads us to conclude that for large NS periods P and typical conversion radii r_c, the frequency shift due to the accelerating plasma is subdominant compared to that from the asymptotic DM velocity dispersion, $\Delta f/f \sim 10^{-6}$. The frequency shift may be at the percent level for neutron stars with millisecond periods, but as shown in Eq. (11) in the main text, our signal is strongest for neutron stars with long periods, and thus will not affect our sensitivity estimates from these targets.